Research Square

Preprints are preliminary reports that have not undergone peer review.
They should not be considered conclusive, used to inform clinical practice,
or referenced by the media as validated information.

Leaching Behaviour of Blended Magnesium Potassium Phosphate Cements

Raphael Margreiter

raphael.margreiter@postgrad.manchester.ac.ul

University of Manchester

Thomas S. Neill

University of Manchester

Sam Shaw

University of Manchester

Katherine Morris

University of Manchester

Article

Keywords: chemically-bonded ceramics, magnesium potassium phosphate cement, 35 radioactive waste disposal, mineralogy, struvite-K

Posted Date: November 12th, 2026

DOI: https://doi.org/10.21203/rs.3.rs-11514268/v1

License: This work is licensed under a Creative Commons Attribution 4.0 International License.
Read Full License

Additional Declarations: No competing interests reported.

Leaching Behaviour of Blended Magnesium Potassium Phosphate Cements

Raphael Margreiter[1*], Thomas S. Neill[1], Sam Shaw[1], Katherine Morris[1*]

[1*]Department of Earth and Environmental Science, The University of Manchester, Oxford Rd, Manchester, M13 9PL, United Kingdom.

*Corresponding author(s). E-mail(s): raphael.margreiter@postgrad.manchester.ac.uk; katherine.morris@manchester.ac.uk;
Contributing authors: thomas.neill@manchester.ac.uk; sam.shaw@manchester.ac.uk;

Abstract

Magnesium Potassium Phosphate Cements (MKPCs) show promise as immobilisation matrices for Depleted, Natural and Low Enriched Uranium (DNLEU) disposal. To this end, their development in contact with and their influence on intruding groundwater is a key area of interest. Finely ground MKPCs blended with either pulverised fly ash (PFA), blast furnace slag (BFS) or with no filler (NF) were leached in deionized water and a disposal relevant synthetic groundwater for up to one year to assess the impact of leaching on cement mineralogy and groundwater evolution. Solid and liquid phases are analysed at seven time points over a month, plus an additional point after a year in select samples by XRD, BET surface area analysis, pH measurements, and ICP-AES. Thermodynamic models where also setup to evaluate the influence of different conditions. While the addition of PFA to MKPC does not significantly affect their phase composition and leaching behaviour compared to the no filler system, systems containing BFS differ strongly from filler free systems. It is shown that in all systems, initial equilibration is completed within 28 days. Leaching in DI has limited effects on the phase composition of the cements, while interaction with synthetic groundwater leads to a large-scale transformation of the main struvite-K binder phase to a mix of hazenite and hydroxyapatite. Leachate pH is strongly affected by the chosen filler and generally higher than previously reported for

MKPC systems (10-13 vs 8-10). Both phosphates and silicates are released into the leachate at low levels.

Keywords: chemically-bonded ceramics, magnesium potassium phosphate cement, radioactive waste disposal, mineralogy, struvite-K

1 Introduction

The internationally favoured approach to the disposal of intermediate and high-level radioactive wastes is deep geological disposal in a Geological Disposal Facility (GDF)[1]. This approach applies a 'multi-barrier system' of engineered barriers in a bespoke, sub-surface facility emplaced at depths of 200-1000 m. The multi-barrier system includes the wasteform (including its conditioning matrix), its container, the backfill used to fill void spaces during closure of the facility, and the host rock, all of which are intended to limit migration of radionuclides for extended periods (tens to hundreds of thousands of years) to ensure no harmful quantities of radioactivity ever reach the biosphere [2]. An intrinsic part of the multi-barrier system is the local backfill/buffer which is intended to both physically and chemically stabilize the wasteform; the latter by 'conditioning' the disposal region to a predictable local pH and solution chemistry and restricting microbial activity [2]. In the UK, the development of suitable backfill materials is part of ongoing work to create a 'toolbox' of functional materials tailored to different radioactive waste disposal scenarios [3–5].

A promising candidate backfill material is Magnesium Potassium Phosphate Cement (MKPC), an acid-base cement originally applied in dentistry before applications expanded into civil engineering and radioactive waste disposal [6–8]. For radioactive waste disposal, MKPC may be relevant as an encapsulant for (reactive) metals in intermediate level waste [9–14] and as a backfill/immobilisation matrix for select wastes, potentially including depleted, natural, and low-enriched

uranium (DNLEU). Here, MKPCs may have beneficial properties compared to Portland Cement (PC) formulations including a reduced CO_2 footprint [15, 16], their corrosion-limiting properties [17, 18] and an increased resistance to certain environmental perturbations including sulphates, radiation and temperature compared to some PC formulations [19, 20].

Intrinsic to MKPC, typically a blend of MgO, KH_2PO_4 and H_2O, is an elevated phosphate concentration in the cement and associated leachates where dissolution of the cement binder phases controls the porewater composition [13]. This makes the material particularly relevant to wastes containing uranium, and potentially transuranics, due to the anticipated formation of poorly soluble phosphates, which may act to retard radionuclide mobility under disposal conditions [21–24]. Determining the equilibrium solution composition and phase transformations of MKPC under a range of leaching conditions is therefore important to explore the potential application of MKPCs in radioactive waste disposal, including deep geological disposal.

Given sufficiently slow reaction rates, MKPC forms through the reaction of MgO and KH_2PO_4 in H_2O as a coherent cementitious network of struvite-K [$MgKPO_4 \cdot 6\,H_2O$](Eq. 1). MKPC forms through intermediate phases ($MgHPO_4 \cdot 7\,H_2O$, $Mg_2KH(PO_4)_2 \cdot 15\,H_2O$) and associated changes in pH and solution composition with an equilibrium porewater pH of 8-10.5 [5, 10, 25–29].

$$MgO_{(s)} + KH_2PO_{4(s)} + 5\,H_2O_{(l)} \longrightarrow MgKPO_4 \cdot 6\,H_2O_{(s)} \tag{1}$$

Commonly used cement formulations utilize excess calcined MgO to reduce reaction rates and ensure full reaction of KH_2PO_4 to struvite-K [9, 30–32]. They also add a retarding agent (commonly boric acid [$B(OH)_3$] [33]) to reduce heat production and

ensure cementation, as well as an inert filler material (e.g. Pulverised Fly Ash (PFA)), to both reduce cost and optimize cement properties [34, 35].

While a variety of studies on the leaching behaviour of Portland-based materials exists (e.g. [36–41]), parallel studies are sparse for MKPC. Of particular note are studies by Torras et al. [13], Lahalle et al. [42], Xu et al. [43], Caselles et al. [44] and modelling work by Lothenbach et al. [26, 45]. All these studies suggest a potential transformation of struvite-K during solution leaching to an amorphous phase with partial substitution of K with Na [42], and bobierrite, $Mg_3(PO_4)_2 \cdot 8\,H_2O$ [13], as well as the release of K, Mg and P into solution.

The aim of this study is to investigate phase changes and variation in leachate compositions in MKPCs as a function of filler and solution composition. To this end, the present work focuses on an experimental matrix comparing the influence of different fillers (without filler (NF), with Pulverised Fly Ash (PFA), and with Blast Furnace Slag (BFS)) and leachates (deionized water and a representative GDF groundwater analogue from the Swiss Mont Terri project [46]) on the present solid phases and solution composition in a setup optimized for rapid equilibration by using finely ground (i.e. high surface area) rather than monolithic cement samples. The cements were leached for up to 28 days with frequent sampling with an additional sampling point after 371 days for both NF systems. Throughout, investigation of phase changes in the leached cements, analysis of the leachates, and comparison with thermodynamic models was used to define the development of the mineral and groundwater chemistry during leaching. This enabled a baseline understanding of MKPC backfill for further investigations into MKPC-radionuclide interactions as potential immobilisation routes in radioactive waste disposal.

2 Results & Discussion

2.1 Cement alteration

The mineralogical development of the cement was investigated through powder XRD analysis. XRD patterns of the individual ground cements with no filler (NF), PFA filler, and BFS filler before and after 28 days leaching in both DI and GW are shown in figure 1, with a complete overview of the patterns at every time point provided in figures C2, C3, and C4 of the extended data.

All XRD patterns for cements prior to leaching showed a MgO reflection at 43° of varying intensity in accordance with the excess MgO in the cement formulation. Cements with PFA filler showed a SiO_2 reflection at 26.5° with a broad amorphous SiO_2 background, consistent with PFA mineralogy, which largely consists of small quartz spheres [47]. Remaining peaks in the PFA and NF systems before leaching, were associated with struvite-K ($MgKPO_4 \cdot 6\,H_2O$) consistent with past work, which determines struvite-K as the stable MKPC phase at pH 8-12 [26, 33, 48]. The pattern from the BFS containing system before leaching was dominated by a mix of calcium silicates in the 30-35° range (larnite [Ca_2SiO_4], hatrurite [$Ca_3(SiO_4)O$]) already present in the BFS filler (see figure B1), and trimagnesium phosphates (e.g.$Mg_3(PO_4)_2 \cdot 5\,H_2O$) at approximately 18.5°, 21°, and 22°. It is noteworthy that struvite-K reflections in the BFS system are of comparatively low intensity, despite being expected to be the main binder phase in MKPC.

For the 28-day samples, leaching in DI did not significantly impact the crystalline phases present in all three cement systems (NF, BFS, PFA) except for a decrease in the MgO peak intensity across all systems, indicating dissolution of MgO over the leaching period. By contrast, leaching in the saline GW (I=0.39M) had a strong influence on the mineral phases observed in the XRD at 28 days. In the no filler and PFA systems, the disappearance of struvite-K and notable emergence of hazenite

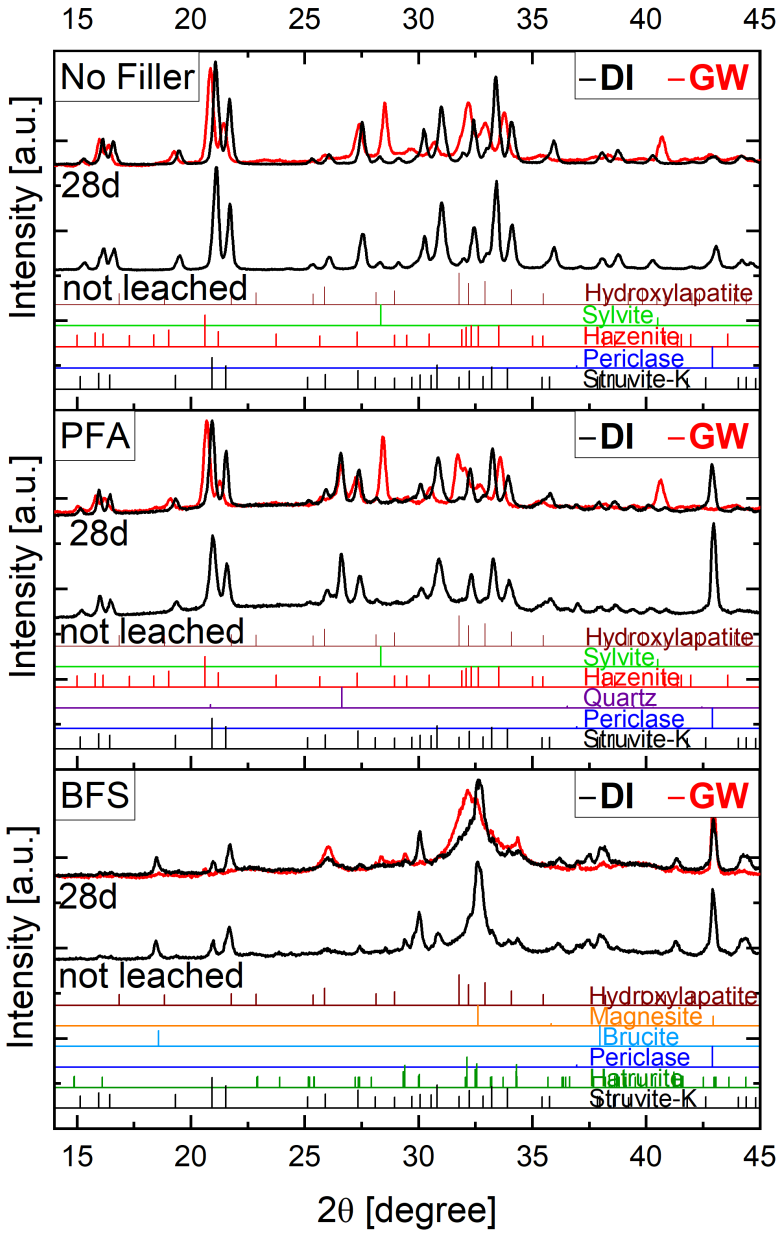


Fig. 1 XRD patterns of MKPCs with different fillers compared to patterns after 28 days leaching in either deionized water (DI) or a disposal relevant groundwater analogue (GW). Patterns are normalized to the highest intensity in the respective XRD patterns.

[$KNaMg_2(PO_4)_2 \cdot 14\,H_2O$] reflections were observed, indicating a partial substitution of potassium with sodium and water in the struvite-K structure. The stability of struvite-K in DI water and the transformation to hazenite in GW were also observed in the NF systems leached with DI and GW for 371 days (see extended data (ED) figure C2). Additionally, in the DI-NF system, struvite-K XRD peaks decreased in width over 28 d aging, suggesting crystallization of the binding phase. In the GW-NF system additional peaks for brucite [$Mg(OH)_2$] appeared in the 371 days sample, suggesting slow formation of crystalline brucite in this system. After 28 days, the diffraction pattern of the GW-BFS system showed a broad reflection at approx. 32° sloping towards a smaller signal at approx. 34°. This is indicative of nanoparticulate hydroxyapatite formation [$Ca_5(PO_4)_3OH$] [49]. A similar, but lower intensity hydroxyapatite feature can be seen in the GW-NF and GW-PFA systems after 28 days. The appearance of the highly soluble sylvite [KCl] in select GW samples may be an artefact of sample preparation where isopropanol washing was not extensive enough to eliminate excess KCl. It is noteworthy that no indication of bobierrite [$Mg_3(PO_4)_2 \cdot 8\,H_2O$] formation is apparent in the XRD patterns, despite it being previously reported [13, 42]. [43] found a similar discrepancy between model-predicted yet experimentally absent bobierrite formation in some systems, and hypothesised that the pH of the leaching solution was a factor wherein lower pH favours bobierrite formation. This agrees with the presented results, where higher pH leachates may have resulted in no bobierrite formation.

In addition to the observed changes in mineralogy, surface area analysis of the cements before and after leaching (see table E1) showed a significant surface area increase in the GW-PFA (2 m^2/g to 55 m^2/g) and GW-NF (2 m^2/g to 76 m^2/g) systems, suggesting significant mineralogical evolution. Interestingly, the magnitude of surface area increase in the GW-PFA system was significantly higher than in the

PFA (filler only) control, suggesting morphological changes in the GW-PFA and GW-NF system were caused by the precipitation of hazenite observed in XRD. Increases in surface area were also seen in the DI-PFA and DI-NF systems presumably due to the pH change from approx. 8 to >10 associated with a potential partial dissolution and following reprecipitation of struvite-K. There were no notable changes in the surface area in the BFS systems despite some evidence for significant calcium hydroxyapatite formation observed in the GW-BFS XRD analysis.

2.2 Leachate development

pH development in all six systems followed simple equilibration curves (see figure 2) over 28 days. Here, both the solution and filler significantly impacted the pH development, with GW experiments showing a lower equilibrium pH than corresponding DI systems, potentially due to buffering associated with the GW solution. BFS filler samples show the highest pH across all time points presumably due to portlandite [$Ca(OH)_2$] dissolution [50], which is formed during hydration of BFS and was observed in the BFS XRD pattern (see ED figure B1) but not in the cement systems. The BFS samples also show the smallest pH change between the 1 h and the 28 d values, demonstrating a rapid initial equilibration rate. The 28 d pH of the BFS and PFA systems seems to be largely determined by the filler material, with the 28 d pH for PFA cement (DI/GW: pH 11.9/10.5) and BFS cement (DI/GW: pH 12.6/12.8) very close to the 28 d pH of filler-only leaching experiments in DI and GW respectively (pure BFS in DI/GW: pH 12.8/12.9, pure PFA in DI/GW: pH 11.6/9.7) (see ED section B). The measured pH values in the current work are higher than the commonly reported equilibrium pH of 8-10 for MKPCs [33], even for the filler free systems. For MKPCs, the equilibrium pH is typically attributed to the buffering effect of $MgO/Mg(OH)_2$. In the current work, it is likely that due to the slow dissolution of calcined MgO, due to calcination and the common ion effect, and the continuous reaction of Mg_2^+ to

183 solid phases other than $Mg(OH)_2$ the pH equilibrium for $Mg(OH)_2$ was not reached
184 at 28 days. A pH of approximately 10 is expected over extended time in the NF sys-
185 tems consistent with $Mg(OH)_2$ equilibration and supported by the lower pH values
186 observed after 371 days (DI-NF: pH 11.5, GW-NF: pH 10.6).

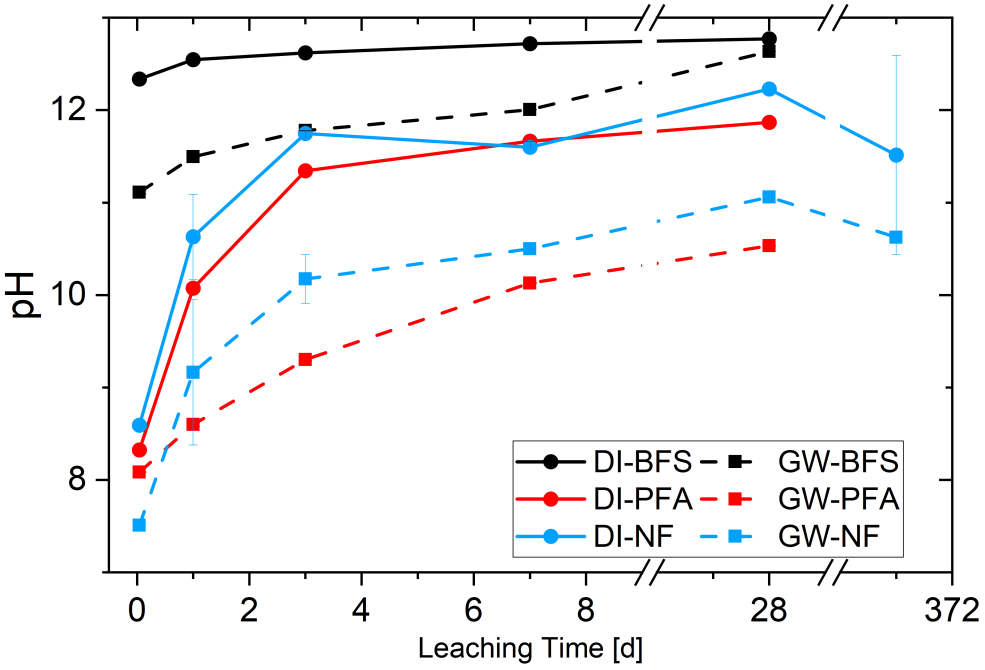


Fig. 2 pH development of leachates of MKPCs with no filler [blue], PFA [red] and BFS [black] filler materials from 1 h to 28 d in deionized water [solid line] or Pearson groundwater [dashed line]. Error bars represent the standard deviation from triplicate experiments. 3 h and 7 h data points omitted for readability.

187 ICP-AES analysis was performed to determine the concentration of key elements
188 in the solution over the experimental duration (see figure 3 and ED D). The phos-
189 phorous concentration is of particular interest in the context of radioactive waste
190 disposal, due to the predicted low solubility of uranium phosphates [21, 23]. Both the
191 NF and the PFA cement systems demonstrate a clear trend of an early phosphorous
192 release at first contact with both DI and GW (up to 25-30 mM in DI and 5-10 mM
193 in GW), followed by a subsequent reduction in soluble phosphorous to concentrations

<1 mM in the first week of leaching. For both cements the initial phosphorous release was higher in the respective DI system than the GW system ([P](DI-PFA): 32 mM vs [P](GW-PFA): 2.6 mM, and [P](DI-NF):25.4 mM vs [P](DI-NF): 9.3 mM; see 3). The observed trend in phosphate concentration correlates with the pH increase discussed above and suggests fast dissolution of more amorphous struvite-K like phases or unreacted KH_2PO_4 under initial circumneutral and slightly alkaline conditions, followed by reprecipitation of struvite-K as the pH rises above 10 over the first week. An indicator for this is the decrease in peak width in struvite-K XRD reflections up until day 3 suggesting ingrowth of this more crystalline phase (see ED figures C2 and C3). It is also noteworthy that the BFS systems, which reached their equilibrium pH within an hour, did not show a similar initial phosphorous release. This is consistent with previous work by [13] where the cumulative P release across systems with a daily refresh of DI solution, i.e. cement kept in persistently circumneutral leaching solution, is much higher than in systems with an identical number of refreshes but multiple days of contact time between them, i.e. where the leaching solution had time to equilibrate to a more alkaline pH. The lower overall phosphorous release to solution in the GW systems is explained by the lower solubility of P due to formation of hazenite [$KNaMg_2(PO_4)_2 \cdot 14\,H_2O$] under conditions where struvite-K is unstable. Once again, the BFS containing systems showed different behaviour to the PFA and no filler systems with clear differences between the respective DI and GW systems. While the DI-BFS system seems to show a saturation of phosphorous in the solution phase at approximately 15 mM after 3 days, the phosphorus concentration in the GW-BFS was low at approximately 1 mM up until day 7 and then increased to 8 mM at day 28, coinciding with the formation of new mineral phases observed in the XRD patterns (e.g. hydroxyapatite).

Magnesium concentrations in the PFA and NF leachates showed similar trends over time. In the DI systems, there was an initial increase in Mg concentration to

4 mM over the first hour, followed by a rapid drop to <0.1 mM by day 1. In the GW systems there was an initial increase to 22 mM over the first hour followed by a gradual downward trend to 5 mM at 28 days. The behaviour in the DI systems mirrored the phosphorous concentrations where initial dissolution of amorphous struvite-K like phases in the first hours was followed by formation of $MgO/Mg(OH)_2$ and more crystalline struvite-K. In contrast to the P concentrations, the initial Mg concentrations in the GW systems (approximately 23 mM) were much higher than in the parallel DI experiments (approximately 5 mM). This is explained by the elevated Mg concentration in the simulated groundwater (approximately 17 mM). In the GW systems, the gradual decrease in Mg solution concentration over 28 days suggests slow formation of a magnesium-rich phase such as brucite, which is observed in select XRD patterns of this system, or amorphous bobierrite-like phases $[Mg_3(PO_4)_2 \cdot 8\,H_2O]$ as observed by [13]. Both BFS systems showed low Mg concentrations at all time points suggesting active scavenging of aqueous Mg to Mg bearing phases (e.g. magnesite $[MgCO_3]$, brucite, bobierrite, and magnesium silicates) was occurring.

The potassium concentrations in solution of the PFA and NF systems were similar throughout leaching. After an initial elevated K release in the first hours of leaching, the K concentration in both DI systems stabilized at approx. 40 mM after a day. The initial peak is explained by dissolution of amorphous struvite-K like phases at circumneutral pH whilst the elevated K concentration throughout leaching suggests an additional source of K in the original cement that is independent from the filler. Here, dissolution of previously unreacted KH_2PO_4 is a likely source of K, although a corresponding increase in solution phosphate concentration is not observed, suggesting additional precipitation of phosphates was occurring in these systems. In both GW systems, there was a continuous potassium release. This correlates well with continual transformation of struvite-K $[MgKPO_4 \cdot 6\,H_2O]$ to hazenite $[KNaMg_2(PO_4)_2 \cdot 14\,H_2O]$ observed in the XRD analysis during which K is released and substituted with Na

in the solid. Both BFS systems follow a broadly similar trend in K solution profiles as the NF and PFA systems, albeit with a slightly longer equilibration time and the final K concentration about twice as high. The broadly similar trends between the GW systems could suggest similar interpretations of a struvite-K to hazenite transformation, although this is not obvious in the XRD patterns potentially due to expected XRD detection limits.

The trend in calcium concentration across all filler types was consistent with rapid equilibration with a low solubility Ca phase, stabilizing at <0.1 mM in DI systems and <1 mM in GW from the first data point, and clearly suggesting the rapid precipitation of a solubility controlling calcium-rich phases. This is in accordance with the rapid formation of hydroxyapatite [$Ca_5(PO_4)_3OH$] clearly observed in the GW-BFS systems and in the GW systems of NF and PFA cement (figure 1). The formation of hydroxyapatite under GW leaching conditions is supported by thermodynamic modelling (see section 2.3).

2.3 Thermodynamic Modelling

The model phase assemblage, i.e. mineral phases allowed to precipitate when oversaturated, was chosen to reflect experimental findings. A noticeable exclusion from the phase assemblage is quartz (SiO_2) which is not included in the model due to the high predicted thermodynamic stability of the $MgSiO_3$(aq) solution species. Including quartz in the model leads to predictions of the near complete dissolution of both quartz and periclase to form $MgSiO_3$(aq), which contradicts the experimental XRD patterns. Also not included in the model is bobierrite ($Mg_3(PO_4)_2 \cdot 8\,H_2O$) which is oversaturated in all modelled experimental systems. Indeed, bobierrite is the thermodynamically stable magnesium phosphate phase predicted in all systems. However, its inclusion in the model leads to prediction of the complete dissolution of struvite-K ($MgKPO_4 \cdot 6\,H_2O$) and hazenite ($KNaMg_2(PO_4)_2 \cdot 14\,H_2O$) phases counter to experimental observations.

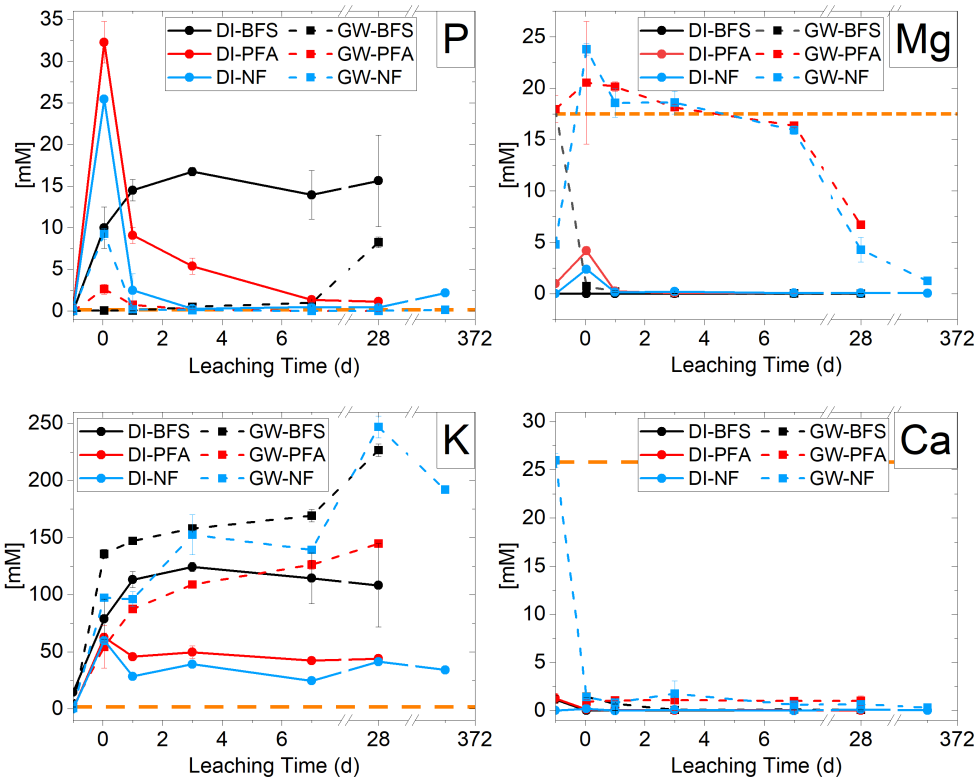


Fig. 3 Development of the elemental concentrations of phosphorous (P), magnesium (Mg), potassium (K), and calcium (Ca) in the leachates of MKPC prepared with different filler materials and leached in either deionized water (DI) or a groundwater analogue from the Swiss Mont Terri project (GW). Data points at t= -1 represent concentrations in DI or GW, respectively. Dashed orange line shows elemental concentrations in GW. Error bars are the standard deviation of triplicates. Concentrations for silicon (Si) and sodium (Na) in ED D.

The thermodynamic models of struvite-K in pure water and GW leaching systems predicts the mineral to be largely stable in pure water (albeit less pronounced in the DI-BFS system) and unstable in GW (see E3). In all GW leaching systems hazenite is predicted to precipitate, albeit only to a limited extent in the BFS system. In the BFS systems, modelling predicts hydroxyapatite as the dominant phosphate phase, which is also predicted to a minor extent in all Ca containing systems. Overall, thermodynamic modelling results predicting hazenite and hydroxyapatite formation are in good agreement with the XRD results (see 1).

Delayed brucite formation is posited as an explanation for the higher-than-expected pH in the experimental systems over the initial 28-day experiment. Indeed, adding brucite as an equilibrium phase into the model (i.e. allowing it to precipitate in the model) leads to a stark drop in the solution pH (see table E4). This reflects the 1-year experimental observation where the appearance of brucite reflections in the XRD correlates with a drop in solution pH, which is consistent with slower (over several months) formation of brucite in these experiments, potentially explained by the common ion effect favouring formation of other Mg-phases over brucite formation.

The elemental concentrations predicted by the model (see table E5) are only an estimation and are not likely to precisely match those of the experimentally determined ones (see table E9). Likely reasons for this are either impurities in the regents that have not been considered in the model, amorphous solid phases not observed in the XRD and therefore not included in the model, and the experimental systems not reaching thermodynamic equilibrium after 28 days. Overall, the model replicates the differences between the DI-NF/PFA and DI-BFS system but is less reliable in the more complex GW leaching experiments where experimental differences between the NF and PFA system are more pronounced. The model overestimates [Mg], particularly for the NF and PFA systems. This is likely explained by precipitation of magnesium phases not included in the model, such as brucite or various magnesium silicates, which become oversaturated when quartz is included in the model phase assemblage. It significantly underestimates [K] and [Na], and slightly [Si], pointing to impurities in the reactants, particularly MgO. The model overestimates [P] in the DI systems and GW-NF, pointing to the formation of additional P phases not found in the XRD, e.g. minor amorphous bobierrite-like phases. Interestingly, the model significantly underestimates [P] in the GW-BFS case which suggests that this increase in P is either a kinetic effect or a general indicator that the model is only able to resolve some aspects of the experimental data.

3 Conclusions

Through a matrix of sacrificial leaching experiments, the alteration of MKPC with different filler materials and the respective leachate evolution in deionized water and a Mont Terri groundwater analogue has been investigated. A system without filler was chosen as a baseline and compared to systems with either 50 mass-% PFA, largely consisting of SiO_2 particles, or 50 mass-% BFS, qualitatively similar in composition to some Portland cement clinkers.

It was demonstrated that both the choice of filler and leaching solution have a pronounced influence on cement and leachate alteration. While deionized water has a limited effect on the mineralogical composition of the cement over 28 days of leaching, with cement before and after leaching consisting mostly of struvite-K and periclase for no filler and PFA systems and calcium silicates and magnesium phosphates in BFS system, leaching with a groundwater analogue leads to the transformation of the main binder phases to a mix of hazenite and hydroxyapatite over 28 days. Hazenite dominated in systems without filler or with PFA filler and hydroxyapatite dominated where BFS was used as the filler, presumably due to the elevated Ca concentration and higher pH of this system. The thermodynamically predicted formation of bobierrite seems to be hindered by kinetic effects and/or influence of pH in the presented experiments consistent with relevant literature [43]. Where bobierrite formation has been reported in literature, the pH equilibration of MKPC with its environment has been artificially prevented by various means keeping the systems circumneutral (e.g. frequent refresh of the eluant). The presence of hydroxyapatite particularly in the GW-BFS system is of note as it is investigated as a barrier for radionuclide migration in remediation efforts of contaminated land [21, 24]. The transformation of struvite-K to hazenite in the GW-NF and GW-PFA systems is accompanied by a significant increase in surface area, potentially increasing the number of potential sorption sites for radionuclides in a disposal scenario.

Leachate pH was observed to be significantly higher than previously reported for MKPCs with pH values ranging from 10-13 depending on the investigated systems. It was demonstrated that the choice of filler strongly influences the expected pH, potentially offering a pathway to adjust the local chemical environment, at least over the short term, by selecting different filler materials. This observed high pH in filler-containing systems is attributed to the slow kinetics of the $MgO/MgOH_2$ buffering system (i.e. slow brucite formation).

The equilibrated leachates show phosphate and silicate concentration in the higher µM range which should be favourable to maintaining low U mobility by precipitating uranium as oversaturated silicate and phosphate phases and low enough to maintain a constant concentration of reactants in the near-field for extended periods.

4 Methods

4.1 Materials

Cements

The MKPC formulation was adapted from [14]. All cements were prepared from magnesium oxide light, MgO (VWR, assay ≥97.0 % [max. 1.5 % silica]), potassium phosphate monobasic, KH_2PO_4 (Sigma-Aldrich, ACS reagent ≥99.0 %), boric acid, $B(OH)_3$ (VWR, AnalaR), and 18.2 MΩ·cm ultrapure water used in ratios shown in table E6. Before use, the MgO was calcined for 6 h at 1300 °C (Carbolite CWF 1300 furnace). The calcined material was milled and the grain size fraction of 53-500 µm, with a resultant surface area of approximately 1.2 m^2/g, was used for the subsequent MKPC formulation (discussion of the influence of calcination and grinding on MgO surface area in ED section A). Three systems were studied: I) MKPC no filler (NF), II) MKPC with PFA filler (PFA; ScotAsh, EN450), and III) MKPC with BFS filler (BFS; Ketton, BN7). Characterization of the filler materials (PFA and BFS) by XRD

is provided in figure B1 of the SI.

Calcined MgO, deionized H_2O, $B(OH)_3$, and, where relevant, filler were manually stirred to a homogeneous mix. KH_2PO_4 was then mixed in using a mechanical stirrer at 270 rpm for 10 mins, then 330 rpm for 20 mins to initiate MKPC formation. The resultant slurry was poured into a cylindrical mould, demoulded after a day, and then cured for at least 28 days at ambient temperature prior to use in experiments. The cured cements were subsequently ground in a steel canister grinder and sieved to select a particle size of 53 µm - 125 µm for leaching experiments [51].

Leaching solutions

Two waters were used in the leaching experiments: I) 18.2 MΩ·cm ultrapure water (DI) and II) a representative, synthetic groundwater (GW) [46] (Table E7) of relevance to radioactive waste disposal. To minimise CO_2 ingress into the experiments, DI water was boiled for 30 mins and then rapidly cooled in an ice bath under constant flow of N_2 [51] with the relevant salt additions for the GW added in a low CO_2 glovebox (box and airlock purged with air pumped through three consecutive 15M NaOH scrubbers, based on [52]).

4.2 Leaching procedure

Batch leaching experiments were performed on the three synthesised cements in a low CO_2 glovebox. For each batch leaching experiment 3 g of ground cement (53 µm - 125 µm) was mixed with 30 mL DI or GW respectively in a 30 mL HDPE Nalgene bottle (based on [53]) and constantly mixed at 120 rpm on an orbital shaker. Experiments were performed in triplicate. Samples were taken at 1 h, 3 h, 7 h, 1 d, 3 d, 7 d, and 28 d (and 371 d for DI-NF and GW-NF) to investigate the equilibration of the cement with different leaching solutions. Blank water samples (DI and GW) as well as filler only samples in water were run as experimental controls. Solids and solutions

were separated by settling for approximately 10 mins and sampling 10 mL of the resultant supernatant with a syringe and filtering through a 0.22 µm syringe filter (13 mm, PES membrane, Kinesis). The remaining solution was decanted and the solid washed once with isopropanol and dried overnight at 40 °C prior to further analysis.

4.3 Analytical Techniques

X-Ray powder Diffraction (XRD) was performed on samples after curing and at select leaching time points (Bruker D2 Phaser with Cu cathode (K_α = 1.54 Å) in a 5°-70°2θ range, 1 s measurement time per 0.02°increment, mounted on an XRD glass slide). The patterns were analysed by comparison with the ICDD PDF-4/Minerals 2024 crystallographic database. Surface area was determined with three measurements per sample using the Brunauer-Emmett-Teller (BET) method (Micrometrics Gemini VII 2390a, N_2 at 77 K) after vacuum sample preparation (Micrometrics VacPrep 061). pH was measured with a Mettler-Toledo InLab Micro Pro-ISM pH electrode with pH meter, routinely calibrated with pH 10.01, 7.01, and 4.01 standard buffer solutions. The pH is calculated from 9 individual measurements (3 each per sample in the triplicate setup), as the mean of the respective hydrogen ion concentrations converted to pH. The given standard deviation is the standard deviation of the individual pH measurements from this mean. The concentration of Na, Mg, Si, K, Ca, P, and S in the leachate was determined on triplicate samples after 1:100 dilution in 2 % HNO_3 using Inductively Coupled Plasma Atomic Emission Spectrometry (ICP-AES, Agilent ICP-OES 5800) calibrated against a multi-element dilution standard.

4.4 Thermodynamic modelling

Experimental results were compared to thermodynamic model representations of the systems using the PHREEQC software package [54], employing the CEMDATA 18.1 database with a phosphate cement extension [26, 45]. The model was supplemented

with periclase (MgO) (from the ThermoChimie11a database [55]), and hazenite ($Mg_2NaK(PO_4)_2 \cdot 14\,H_2O$) with the solubility product logK=24±2 from an estimation by [43].

To develop the thermodynamic modelling approach, it was necessary to select a phase assemblage that would provide realistic model outputs. The selection of this assemblage (see table E2) is explained in 2.3. The phase assemblage was set to equilibrium with 10 moles of the respective waters (pure water and GW).

Data availability

All data generated or analysed during this study is included in this published article and its extended data. Raw data will be made available from the corresponding author on reasonable request.

Author Contribution Statement

Conceptualization, R.M.,K.M.,T.N. and S.S.; Methodology, R.M.,K.M.,T.N. and S.S.; Validation, R.M.,K.M.,T.N. and S.S.; Formal analysis, R.M.; Investigation, R.M.; Resources, K.M. and S.S.; Data curation, R.M.; Writing - original draft preparation, R.M.; Writing - review and editing, K.M.,T.N. and S.S.; Visualization, R.M.; Supervision, K.M.; Project administration, K.M. and T.N.; Funding acquisition, K.M. and T.N.. All authors have read and approved the final manuscript.

Acknowledgements

This work was funded by Nuclear Waste Services (NWS, grant NWS-UoM-07) through its Research Support Office and is a product of independent academic research and does not constitute or establish an NWS position. Any review of this work by NWS was limited to ensuring the appropriate use of NWS terminology, or to provide a general review of the scientific method. This research utilized the RADER National Nuclear

User Facility at the University of Manchester, established with financial support from EPSRC and BEIS, under grant number EP/T011300/1. T. Neill acknowledges EPSRC for funding under the EP/X036065/1 fellowship grant. The authors thank Dr. Anthony Stockdale from the RADER NNUF for technical support, and Dr. Roseanna Byrne and Dr. Abby Ragazzon-Smith from the Manchester Analytical Geochemical Unit (MAGU) for analytical support.

Declarations

All authors declare no financial or non-financial competing interests.

Appendix A Extended Data: Calcination

After a variety of small-scale tests, 1300 °C for 6 h was selected as the most practicable calcination condition for MgO. With smaller grain sizes desirable for an even distribution of MgO throughout the sample, a series of tests were performed to determine the influence of grinding, sieving, and grain size on the surface area of the MgO. This test series consisted of three MgO batches, one uncalcined, the other two calcined at 1300 °C for 6 h. The calcined samples were broken up after burning them in the furnace, ground and sieved, the uncalcined sample was only sieved. BET measurements were performed on every grain size fraction (<53 µm, 125-53 µm, 500-125 µm, >500 µm) as well as the whole batch ("As Is" and "Ground") without grain size selection. Results are shown in table E8.

While calcination significantly alters the surface area of MgO, grinding and sieving show no noteworthy effect. This suggests that grains are rather porous agglomerations of even smaller particles with the respective surface area. Considering these results, the grain size fraction from 500-53 µm was selected for the cement preparation. The reasoning behind this selection was that larger grain sizes might negatively affect the

homogeneity of the cement paste, and that smaller grains might show unexpected behaviours due to the possibility of actually breaking up the agglomerating particles.

Appendix B Extended Data: Filler

Figure B1 show the XRD patterns of the pure PFA and BFS used in this experiment and their patterns after 28 days in the relevant waters. The PFA patterns show quartz, SiO_2, as the main component with mullite, $2.15\,Al_2O_3 \cdot SiO_2$, as secondary phase and traces of magnesite, $MgCO_3$. The pattern does not significantly change during leaching, except for a slight signal broadening in the DI water sample and the presence of halite, NaCl, in the GW sample, likely an artefact from sample preparation. BFS is a mix of calcium silicates (hatrurite Ca_3SiO_5, larnite, Ca_2SiO_4, and merwinite, $Ca_3MgISiO_4)_2$) and calcite ($CaCO_3$). It is noteworthy that hatrurite and larnite are also the main components in Portland cement clinker (as alite and belite). After leaching in both waters, portlandite ($CaCO_3$) reflections dominate the pattern with the intensity ratios of 21° and 34° suggesting a preferred orientation in the 001 direction.

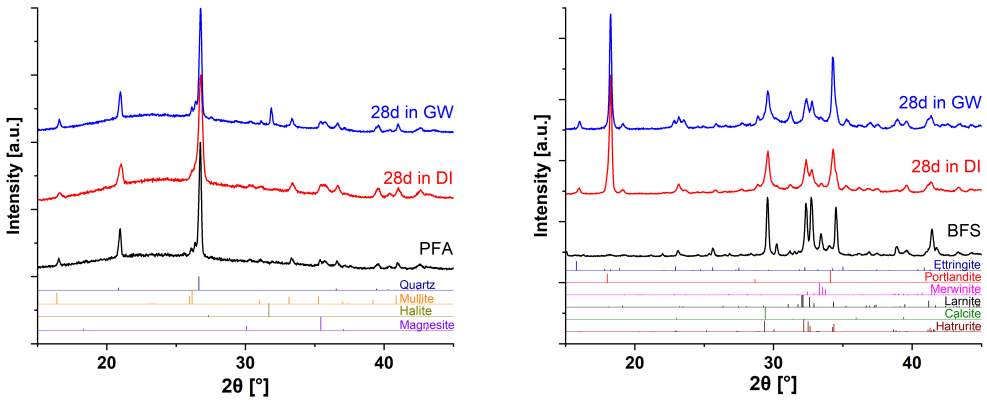


Fig. B1 XRD patterns of blast furnace slag (top) and pulverised fly ash (bottom) before and after storing it for 28d in DI water and a groundwater analogue (GW), respectively.

Appendix C Extended Data: Leached MKPC XRD

The gradual evolution of struvite-K to hazenite in both the GW-PFA and GW-NF system is particularly clear in the area from 20° to 22°. The two struvite-K signals at 21° and 21.5°, steadily loose intensity throughout the first 24 hours, with the two hazenite signals at 20.7° and 21.25° steadily gaining intensity.

The phase transformations in the GW-BFS system happens relatively slow, with the most obvious changes appearing between the 7d and 28d sample.

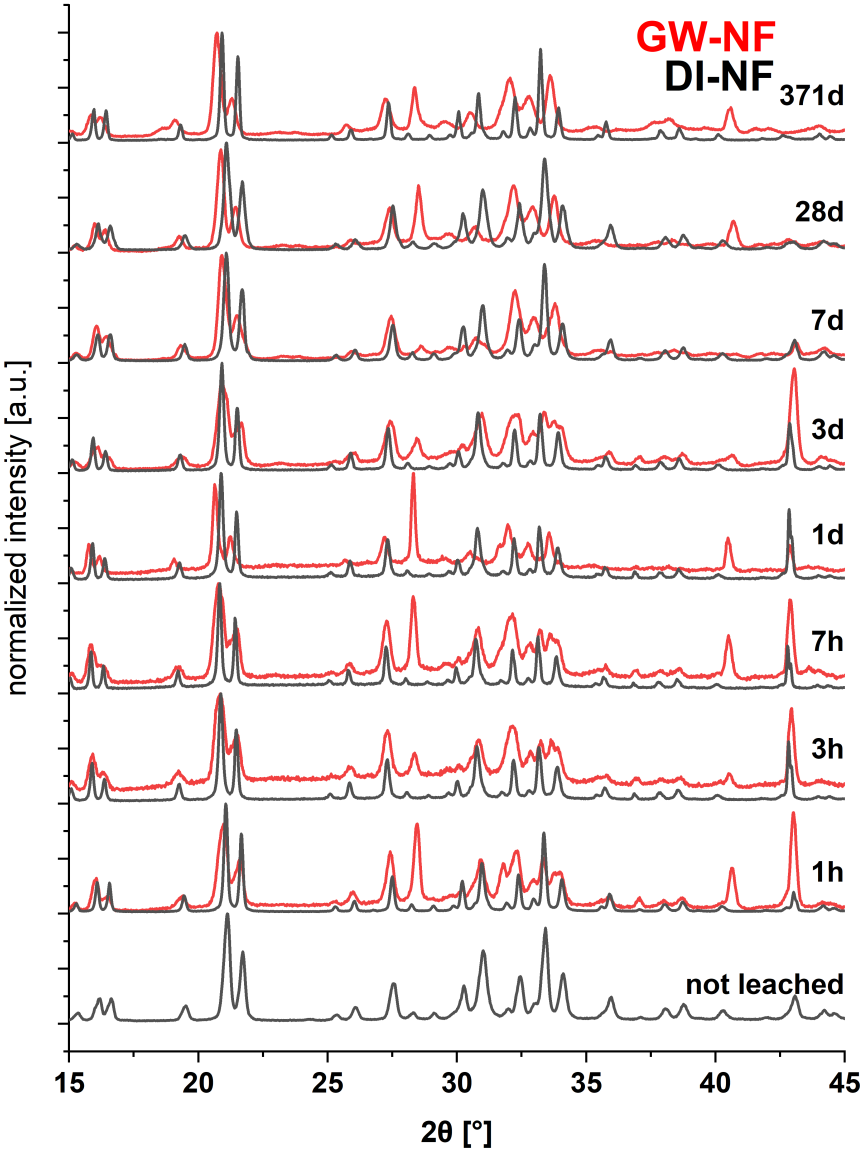


Fig. C2 Development of XRD patterns of MKPC prepared without a filler material leached over a 28d period in DI water (black) and a groundwater analogue (GW) (red). Samples were taken after 1h, 3h, 7h, 1d, 3d, 7d, 28d and 371d in the respective medium. For better reflection comparison, patterns are normalized to the highest intensity in the respective pattern.

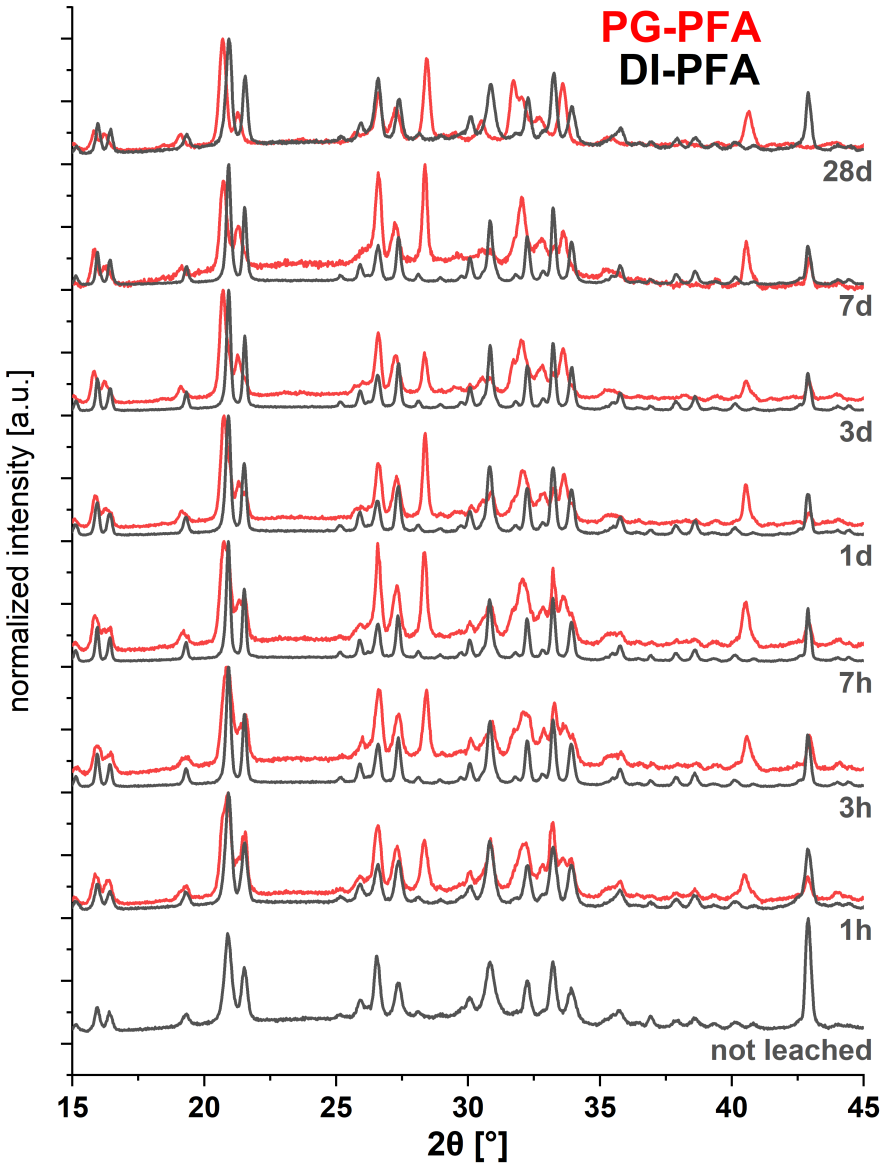


Fig. C3 Development of XRD patterns of MKPC prepared with a pulverised fly ash filler, leached over a 28d period in DI water (black) and a groundwater analogue (red). Samples were taken after 1h, 3h, 7h, 1d, 3d, 7d and 28d in the respective medium. For better reflection comparison, patterns are normalized to the highest intensity in the respective pattern.

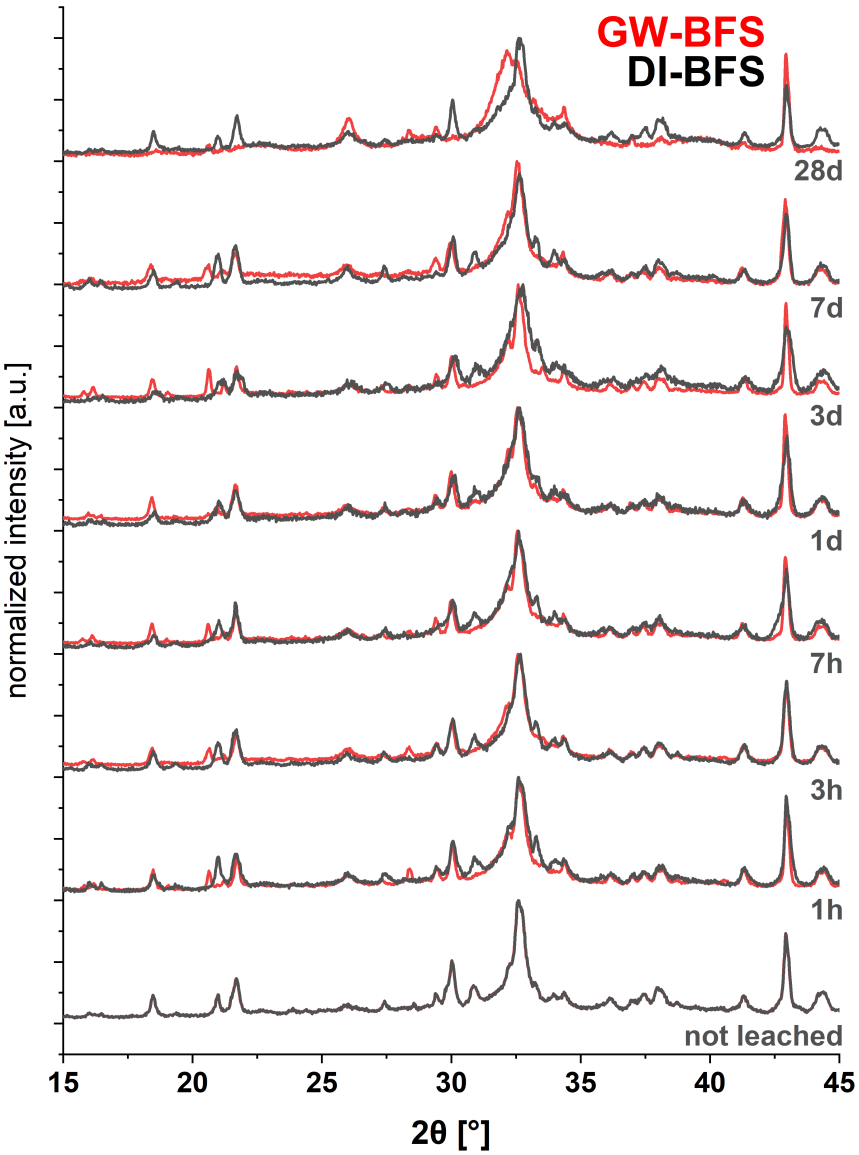


Fig. C4 Development of XRD patterns of MKPC prepared with a blast furnace slag filler, leached over a 28d period in DI water (black) and a groundwater analogue (red). Samples were taken after 1h, 3h, 7h, 1d, 3d, 7d and 28d in the respective medium. For better reflection comparison, patterns are normalized to the highest intensity in the respective pattern.

Appendix D Extended Data: ICP-AES

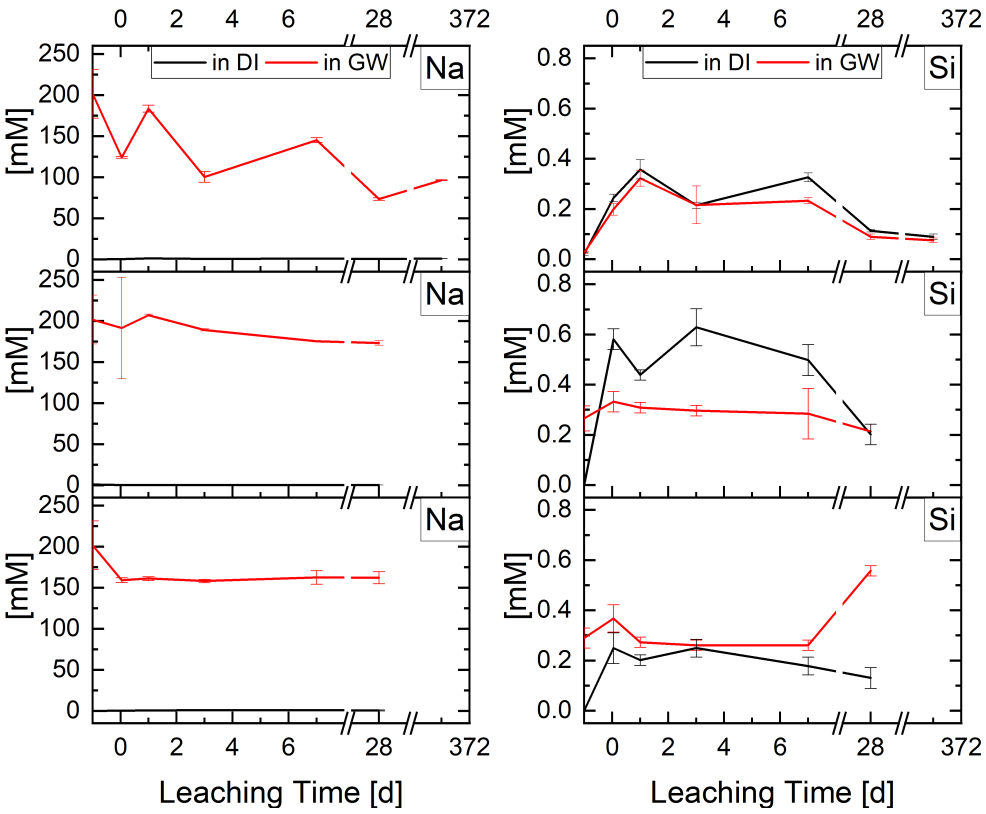


Fig. D5 Development of the elemental concentrations of silicone (SI), and sodium (Si) in the leachates of immobilisation prepared with different filler materials and leached in either deionized water (DI, black line) or a groundwater analogue from the Swiss Mont Terri project (GW, red line). (Mind the x-axis break from 8 to 27 days and 30 to 370 days)

References

[1] NEA. Moving forward with geological disposal of radioactive waste. Report 6433 (2008).

[2] Marsh, A. I., Williams, L. G. & Lawrence, J. A. The important role and performance of engineered barriers in a uk geological disposal facility for higher activity

radioactive waste. *Prog. Nucl. Energy* **137**, 103736 (2021).

[3] Milestone, N. B. Reactions in cement encapsulated nuclear wastes: need for toolbox of different cement types. *Adv. Appl. Ceram.* **105**, 13–20 (2006).

[4] Lee, W. E., Gilbert, M., Murphy, S. T. & Grimes, R. W. Opportunities for advanced ceramics and composites in the nuclear sector. *J. Am. Ceram. Soc.* **96**, 2005–2030 (2013).

[5] Hayes, M. & Godfrey, I. H. Development of the use of alternative cements for the treatment of intermediate level waste. *Waste Management Symposium* **7** (2007).

[6] Wilson, A. D. & Nicholson, J. W. *Acid-Base Cements: Their Biomedical and Industrial Applications* Chemistry of Solid State Materials (Cambridge University Press, Cambridge, 1993).

[7] Qiao, F. *Reaction Mechanisms of Magnesium Potassium Phosphate Cement and its Application*. Thesis (2010).

[8] Wagh, A. S. *Chemically bonded phosphate ceramics: twenty-first century materials with diverse applications (Second Edition)* (Elsevier, 2016).

[9] Montague, W. *The suitability of magnesium phosphate cement for uranium metal encapsulation*. Thesis (2014).

[10] Wagh, A. S., Singh, D., Jeong, S. Y. & Strain, R. V. Ceramicrete stabilization of low-level mixed wastes-a complete story. Report, Argonne National Lab. (1997).

[11] Buj, I., Torras, J., Rovira, M. & de Pablo, J. Leaching behaviour of magnesium phosphate cements containing high quantities of heavy metals. *J. Hazard. Mater.* **175**, 789–794 (2010).

[12] Singh, D., Ganga, R., Gaviria, J. & Yusufoglu, Y. Secondary waste form testing : ceramicrete phosphate bonded ceramics. Report (2011).

[13] Torras, J., Buj, I., Rovira, M. & de Pablo, J. Semi-dynamic leaching tests of nickel containing wastes stabilized/solidified with magnesium potassium phosphate cements. *J. Hazard. Mater.* **186**, 1954–1960 (2011).

[14] Gardner, L. J. *et al.* Early age hydration and application of blended magnesium potassium phosphate cements for reduced corrosion of reactive metals. *Cem. Concr. Res.* **143**, 106375 (2021).

[15] Chau, C. K., Qiao, F. & Li, Z. Microstructure of magnesium potassium phosphate cement. *Constr. Build. Mater.* **25**, 2911–2917 (2011).

[16] Walling, S. A. & Provis, J. L. Magnesia-based cements: A journey of 150 years, and cements for the future? *Chem. Rev.* **116**, 4170–4204 (2016).

[17] Wang, W.-C., Xue, J.-C. & Huang, W.-H. Study of engineering properties of low-ph self-compacting concrete for concrete plug. *Case Stud. Constr. Mater.* **16**, e01060 (2022).

[18] Jun, L., Yongsheng, J. & Zhishan, X. Corrosion behavior of reinforcing bar in magnesium phosphate cement based on polarization curve. *Sādhanā* **45**, 27 (2020).

[19] Gardner, L. J. *Assessment of magnesium potassium phosphate cements for radioactive waste encapsulation.* Thesis (2016).

[20] Yang, B., Ji, R.-J., Lan, Q., Yang, J.-M. & Xu, J. Sulfate freeze and thaw resistance of magnesium potassium phosphate cement mortar. *Materials* **15** (2022).

[21] Fuller, C. C., Bargar, J. R., Davis, J. A. & Piana, M. J. Mechanisms of uranium interactions with hydroxyapatite: implications for groundwater remediation. *Environ. Sci. Technol.* **36**, 158–65 (2002).

[22] Suzuki, Y., Sato, T., Isobe, H., Kogure, T. & Murakami, T. Dehydration processes in the meta-autunite group minerals meta-autunite, metasaléeite, and metatorbernite. *Am. Mineral.* **90**, 1308–1314 (2005).

[23] Lobeck, H. L. *et al.* Dissolution of poorly soluble uranyl phosphate phases in the metaautunite subgroup under uranyl peroxide cage cluster forming conditions. *Am. Mineral.* **105**, 182–193 (2020).

[24] Robinson, C., Shaw, S., Lloyd, J. R., Graham, J. & Morris, K. Phosphate (bio)mineralization remediation of (90)sr-contaminated groundwaters. *ACS ES T Water* **3**, 3223–3234 (2023).

[25] Covill, A., Hyatt, N. C., Hill, J. & Collier, N. C. Development of magnesium phosphate cements for encapsulation of radioactive waste. *Adv. Appl. Ceram.* **110**, 151–156 (2011).

[26] Lothenbach, B., Xu, B. & Winnefeld, F. Thermodynamic data for magnesium (potassium) phosphates. *Appl. Geochem.* **111**, 104450 (2019).

[27] Chau, C. K., Qiao, F. & Li, Z. Potentiometric study of the formation of magnesium potassium phosphate hexahydrate. *J. Mater. Civ. Eng.* **24**, 586–591 (2012).

[28] Zhen, S., Dong, X., Appiah-Sefah, G., Pan, M. & Zhou, D. Analysis of changes in hydration products during solidification/stabilization process of heavy metals in the presence of magnesium potassium phosphate cement. *J. Appl. Sci. Eng.* **17**, 413–421 (2014).

[29] Lahalle, H. *et al.* Investigation of magnesium phosphate cement hydration in diluted suspension and its retardation by boric acid. *Cem. Concr. Res.* **87**, 77–86 (2016).

[30] Wang, A.-J., Zhang, J., Li, J.-M., Ma, A.-B. & Liu, L.-T. Effect of liquid-to-solid ratios on the properties of magnesium phosphate chemically bonded ceramics. *Mater. Sci. Eng. C* **33**, 2508–2512 (2013).

[31] Ma, H. & Xu, B. Potential to design magnesium potassium phosphate cement paste based on an optimal magnesia-to-phosphate ratio. *Mater. Des.* **118**, 81–88 (2017).

[32] Le Rouzic, M., Chaussadent, T., Stefan, L. & Saillio, M. On the influence of mg/p ratio on the properties and durability of magnesium potassium phosphate cement pastes. *Cem. Concr. Res.* **96**, 27–41 (2017).

[33] Lahalle, H. *et al.* Influence of the w/c ratio on the hydration process of a magnesium phosphate cement and on its retardation by boric acid. *Cem. Concr. Res.* **109**, 159–174 (2018).

[34] Wagh, A. S., Jeong, S.-Y. & Singh, D. High strength phosphate cement using industrial byproduct ashes. *Proceedings of the 1st International Conference on High Strength Concrete* 542–553 (1997).

[35] Dieguez, M. *et al.* Evaluation of fillers for magnesium potassium phosphate cement (mkpc) for the encapsulation of low and intermediate level metallic radioactive wastes. *Materials* **16**, 679 (2023).

[36] Berner, U. R. Evolution of pore water chemistry during degradation of cement in a radioactive waste repository environment. *Waste Manag.* **12**, 201–219 (1992).

[37] Butcher, E. J., Borwick, J., Collier, N. & Williams, S. J. Long term leachate evolution during flow-through leaching of a vault backfill (nrvb). *Mineral. Mag.* **76**, 3023–3031 (2012).

[38] Ochs, M., Mallants, D. & Wang, L. *Radionuclide and metal sorption on cement and concrete* Vol. 2 (Springer, 2016).

[39] Lu, H., Wei, F., Tang, J. & Giesy, J. P. Leaching of metals from cement under simulated environmental conditions. *J. Environ. Manag.* **169**, 319–327 (2016).

[40] Hartwich, P. & Vollpracht, A. Influence of leachate composition on the leaching behaviour of concrete. *Cem. Concr. Res.* **100**, 423–434 (2017).

[41] Heath, T., Schofield, J. & Shelton, A. Understanding cementitious backfill interactions with groundwater components. *Appl. Geochem.* **113**, 104495 (2020).

[42] Lahalle, H., Patapy, C., Glid, M., Renaudin, G. & Cyr, M. Microstructural evolution/durability of magnesium phosphate cement paste over time in neutral and basic environments. *Cem. Concr. Res.* **122**, 42–58 (2019).

[43] Xu, B., Coumes, C. C. D., Lambertin, D. & Lothenbach, B. Compressive strength and hydrate assemblages of wollastonite-blended magnesium potassium phosphate cements exposed to different ph conditions. *Cem. Concr. Compos.* **143**, 105255 (2023).

[44] Diaz Caselles, L. *et al.* Chemical degradation of magnesium potassium phosphate cement pastes during leaching by demineralized water: Experimental investigation and modeling. *Cem. Concr. Res.* **178**, 107456 (2024).

[45] Lothenbach, B. *et al.* Cemdata18: A chemical thermodynamic database for hydrated portland cements and alkali-activated materials. *Cem. Concr. Res.* **115**,

472–506 (2019).

[46] Pearson, F. Artificial waters for use in laboratory and field experiments with opalinus clay. Report, Paul Scherrer Institut TM (1998).

[47] Standards, B. En 450-1, fly ash for concrete—definition, specifications and conformity criteria (2012).

[48] Le Rouzic, M., Chaussadent, T., Platret, G. & Stefan, L. Mechanisms of k-struvite formation in magnesium phosphate cements. *Cem. Concr. Res.* **91**, 117–122 (2017).

[49] Bulanov, E. N., Boldin, M. S., Knyazev, A. V., Korokin, V. Z. & Popov, A. A. Obtaining ceramic materials from hydroxyapatite using spark-plasma sintering. *High Temp. Mater. Process.* **37**, 613–617 (2018).

[50] Ochs, M., Mallants, D. & Wang, L. *Cementitious Materials and Their Sorption Properties*, 5–16 (Springer International Publishing, Cham, 2016).

[51] Alonso, M. C., Garcia Calvo, J. L. & Walker, C. Development of an accurate ph measurement methodology for the pore fluids of low ph cementitious materials. Report 1402-3091 (2012).

[52] Smith, K. *Radionuclide behaviour in hyperalkaline systems relevant to geological disposal of radioactive waste*. Thesis (2014).

[53] Kosson, D. S., van der Sloot, H. A., Sanchez, F. & Garrabrants, A. C. An integrated framework for evaluating leaching in waste management and utilization of secondary materials. *Environ. Eng. Sci.* **19**, 159–204 (2002).

[54] Parkhurst, D. L. & Appelo, C. A. J. Description of input and examples for phreeqc version 3: a computer program for speciation, batch-reaction, one-dimensional

transport, and inverse geochemical calculations. Report 6-A43 (2013).

[55] Madé, B. *et al.* Recent developments in thermochimie – a thermodynamic database used in radioactive waste management. *Appl. Geochem.* **180**, 106273 (2025).

5 Tables

Table E1 BET surface area in m^2/g before and after leaching of cements with either pulverised fly ash (PFA), blast furnace slag (BFS) or no filler (NF) in deionized water (DI) and a Mont Terri groundwater analogue (GW). Values with uncertainty are means of triplicate, without uncertainty are single measurements.

Leaching Time	PFA [Filler only]	DI-PFA	GW-PFA	BFS [Filler only]	DI-BFS	GW-BFS	DI-NF	GW-NF
0 d	1.8	1.0(7)	2(2)	0.9	10(3)	10(6)	1.68(3)	1.68(3)
28 d	6.8	18	51(11)	17.5	10(3)	9.4(5)	29(2)	76(6)

Table E2 Phase assemblage of the respective cement systems in the thermodynamic model. All presented phases have a saturation index of 0.0.

Mineral name	Mineral name	Moles of mineral in phase assemblage		
		NF-MKPC	PFA-MKPC	BFS-MKPC
Periclase	MgO	0.7	0.7	0.9
Struvite-K	$MgKPO_4 \cdot 6\,H_2O$	1	1	1
Hazenite	$KNaMg_2(PO_4)_2 \cdot 14\,H_2O$	0	0	0
Hydroxyapatite	$Ca_5(PO_4)_3OH$	0	0	0
Lime	CaO	0	0	1.3
Boric acid	$B(OH)_3$	0.09	0.09	0.09

Table E3 Thermodynamically modelled solid phase composition of a leaching system of 1 mol MKPC with different fillers in 10 moles pure water and a groundwater analogue.

Mineral name	Mineral formula	DI-NF	DI-PFA	DI-BFS	GW-NF	GW-PFA	GW-BFS
		Moles of mineral in phase assemblage					
Periclase	MgO	0.52	0.52	1.65	0.44	0.44	1.83
Struvite-K	$MgKPO_4 \cdot 6\,H_2O$	0.99	0.99	0.22	0.00	0.00	0.00
Hazenite	$KNaMg_2(PO_4)_2 \cdot 14\,H_2O$	0.00	0.00	0.00	0.42	0.42	0.03
Hydroxyapatite	$Ca_5(PO_4)_3OH$	0.00	0.00	0.26	0.05	0.05	0.31
Lime	CaO	0.00	0.00	0.00	0.00	0.00	0.00
Boric acid	$B(OH)_3$	0.00	0.00	0.00	0.00	0.00	0.00

Table E4 Comparison of the modelled pH for relevant leaching systems with and without brucite ($Mg(OH)_2$) precipitation and the experimentally determined pH after 28 days.

system	pH		
	w/ brucite	w/o brucite	experimental
DI-NF	9.8	12.1	12.2
DI-PFA	9.8	11.1	11.9
DI-BFS	12.4	12.8	12.8
GW-NF	9.4	11.9	10.7
GW-PFA	9.4	11.9	10.5
GW-BFS	10.3	12.2	12.6

Table E5 Thermodynamically modelled solution composition of a leaching system of 1 mol MKPC with different fillers in 10 moles deionized water and a groundwater analogue. Values in square brackets are the elemental concentrations in the experimental systems determined through ICP-MS.

Element	DI-NF	DI-PFA	DI-BFS	GW-NF	GW-PFA	GW-BFS
	Element concentration [mM]					
Ca	0.0 [0.1]	0.0 [0]	0.0 [0]	0.0 [0.7]	0.0 [1]	0.0 [0.1]
K	2.6 [41.3]	2.6 [44]	99.3 [110]	59.4 [250]	59.4 [145]	97.8 [227]
Mg	5.2 [0.1]	5.2 [0.1]	0.0 [0]	38.8 [4]	38.8 [6.7]	0.7 [0.01]
Na	0.0 [0.5]	0.0 [0.3]	0.0 [0.2]	198.5 [74]	198.5 [173]	235.8 [162]
P	2.6 [0.4]	2.6 [1.1]	21.9 [16]	0.0 [0.03]	0.0 [0.01]	0.1 [8.3]
Si	0.0 [0.1]	0.0 [0.2]	0.0 [0.1]	0.1 [0.1]	0.1 [0.2]	0.1 [0.6]

Table E6 Magnesium potassium phosphate cement formulation optimized for the use in a geological disposal context. F: *Filler*, S: *all solids combined*, m: molar ratio, w: weight ratio

	m $\frac{MgO}{KH_2PO_4}$	m $\frac{H_2O}{KH_2PO_4}$	w $\frac{H_2O}{MgO+KH_2PO_4}$	w $\frac{B(OH)_3}{MgO}$	w $\frac{F}{MgO+KH_2PO_4+H_2O}$	w $\frac{H_2O}{S}$
with filler	1.7	5.1	0.45	0.08	0.5	0.26
no filler	1.7	5.1	0.45	0.08	-	0.44

Table E7 Composition of the groundwater simulant used in this research. Given as the elemental molar concentration and the respective compound mass concentrations taken from [46].

	Mass [g/L]		Concentrations [mmol/L]
NaCl	12.4	Na	240
KCl	0.12	K	1.6
$MgCl_2 \cdot {}_6H_2O$	3.46	Mg	17.0
$CaCl_2 \cdot {}_2H_2O$	3.79	Ca	25.8
$SrCl_2 \cdot {}_6H_2O$	0.14	Sr	0.9
Na_2SO_4	2.00	CO_3/HCO_3	0.5
$NaHCO_3$	0.04	SO_4	14.1
		Cl	301
		ionic strength I	*0.39M*

Table E8 BET surface area of different grain sizes of calcined and uncalcined MgO. Calcined 1 and 2 were calcined for 6 h at 1300 °C. For Calcined 2 grains with a size >500 µm were ground until they passed the respective sieve. "As Is": MgO as delivered or roughly broken up after calcination; "Ground": Calcined MgO after single rigorous grinding with pestle and mortar without sieving. Remaining: Upper/lower sieve mesh sizes for this grain size fraction.

	Uncalcined		**Calcined 1**		**Calcined 2**	
	mass ratios	BET surface area [m^2/g]	mass ratios	BET surface area [m^2/g]	mass ratios	BET surface area [m^2/g]
As Is	n/a	38.7 ± 0.3	n/a	1.250 ± 0.006	n/a	n/a
Ground	n/a	n/a	n/a	1.218 ± 0.006	n/a	n/a
>500 µm	0.03	39.7 ± 0.3	0.50	1.189 ± 0.005	n/a	n/a
500 - 125 µm	0.60	39.3 ± 0.3	0.35	1.248 ± 0.007	0.61	1.200 ± 0.005
125 - 53 µm	0.31	39.7 ± 0.3	0.09	1.251 ± 0.004	0.25	1.188 ± 0.008
<53 µm	0.06	40.6 ± 0.3	0.06	1.185 ± 0.005	0.14	1.185 ± 0.009

Table E9 Overview of the leachate composition after 28 days of leaching of an MKPC prepared with BFS-, PFA- or no filler in either deionized water (DI) or a groundwater analogue (GW).

	DI-NF	DI-PFA	DI-BFS	GW-NF	GW-PFA	GW-BFS
pH	12.2	11.9	12.8	11.1	10.5	12.6
B [mM]	9.2	23	7	4.6	6.7	10.8
Ca [mM]	0.14	0	0	0.67	1	0.07
K [mM]	41.3	44	110	250	145	227
Mg [mM]	0.09	0.08	0	4	6.7	0.01
Na [mM]	0.54	0.29	0.2	74	173	162
P [mM]	0.44	1.1	16	0.03	0.01	8.3
S [mM]	0.2	4.1	12	15	21.7	33
Si [mM]	0.11	0.2	0.13	0.09	0.2	0.56